Current-voltage asymmetries and negative differential conductance due to strong electron correlations in double quantum dots

J. Fransson[1,2,3,*] and O. Eriksson[2]
[1]*Department of Materials Science and Engineering, Royal Institute of Technology (KTH), SE-100 44 Stockholm, Sweden*
[2]*Physics Department, Uppsala University, Box 530, SE-751 21 Uppsala, Sweden*
[3]*NORDITA, Blegdamsvej 17, DK-2100 Copenhagen, Denmark*
(Received 10 March 2004; published 6 August 2004)

A theory for asymmetric current-voltage characteristics, in particular negative differential conductance, for double quantum dots with strongly correlated electron states is formulated. By expressing the double quantum dot in terms of its many-body eigenstates, a diagrammatic technique for Hubbard operator nonequilibrium Green's functions is employed. The Green's function for the double quantum dot is calculated beyond mean field theory, and it is found that the spectral weights of the conductive transitions in the double quantum dot redistribute dynamically (bias voltage dependent). The resulting asymmetric current-voltage characteristics and negative differential conductance is discussed in terms of the relative level spacing in the two quantum dots and the hopping rate between the quantum dots. Numerical results of the current-voltage characteristics are presented and compared to experiments.

DOI: 10.1103/PhysRevB.70.085301 PACS number(s): 73.23.−b, 73.63.−b, 72.10.−d

I. INTRODUCTION

Experimental current-voltage (J-V) characteristics of mesoscopic quantum systems, e.g., quantum dots (QDs), double quantum dots (DQDs), coupled carbon nano-tubes (CNTs), or quantum wires, etc., often show a more or less pronounced asymmetry, with respect to the bias voltage.[1–3] Typically these observations are made for man-made nanodevices where one part typically has a complex electronic structure and conductivity (interacting region), that is coupled to two, or more, noncomplex regions (contacts or reservoirs). The complex J-V characteristics becomes particularly apparent in systems where the interacting region is asymmetrically coupled to the left and right contacts. Such asymmetries are frequently argued to be effects of impurities introduced during the growth process or differences in interface roughness of the oxide layers between the contacts and the interacting region.[4,5] Another mechanism that may introduce asymmetries in the J-V, or differential conductance (dJ/dV), characteristics are unintentional background charges which additionally contribute a charging energy to the interacting region.[5] A third argument that has been suggested is that a higher collector barrier enhances the charge storage in the well substantially, thus being responsible for different current amplitudes for the back- and forward-biased device.[6,7] Theoretically, it has been suggested that inelastic scattering, especially for asymmetric structures, gives different contributions in the backward- and forward-bias direction.[8,9] However, a full understanding of the mechanisms responsible for the observed asymmetries in the J-V (dJ/dV) characteristics has not yet been put forward.

Recent experiments on double quantum dots (DQDs) coupled to metallic contacts show, unexpectedly, asymmetric negative differential conductance (NDC) behavior in the current-voltage (J-V) characteristics.[10] The J-V characteristics were asymmetric in the sense that the NDC appeared only in one half of the bias voltage range $(-V,V)$. Features of NDC normally occur in semiconductor double- and multibarrier structures[11,12] and can then be referred to as band-edge effects.[13,14] Transport experiments on DQDs fabricated from semiconductor hetero-structures have displayed sharp resonant peaks[15] which are related to the energy distance between the levels in the two QDs approaches zero. This in turn, creates a resonant state in the DQD.[16] Alignments of the levels in the two QDs, however, are expected to create symmetric J-V characteristics having sharp resonant peaks with large peak-to-valley ratios, in contrast to the observations in Ref. 10. Thus, when the interacting region, e.g., DQD, is coupled to metallic contacts, having a conduction band width of the order of electron volts, such explanations have to be discarded. Normally, one expects that the current should increase with increasing bias voltage, possibly with plateaux due to the zero-dimensional confined energy levels of the interacting region. The NDC observed in Ref. 10 was suggested to be an effect of resonant tunneling between the discrete levels in each dot, although the details of the process are not specified.[10] Furthermore, the observed asymmetric appearance of the NDC is hitherto an unexplained effect.

There is a vast literature of theoretical studies on transport through DQD in different geometries, e.g., DQD in series[17,18] and in parallel.[18–20] Most of these studies are devoted to DQDs in the Coulomb blockade regime, where especially phenomena related to Kondo-like physics are under focus. Although being important for the understanding of effects from strong correlations on the transport through the system, to our knowledge, no-one has yet addressed the question of J-V (dJ/dV) asymmetries or asymmetric NDC in DQDs coupled to metallic contacts.

In this paper we propose a theory that ties these two effects together. By studying an idealized DQD, with one conducting level in each QD, in terms of the eigenstates of the DQD in the atomic limit, we find that the J-V (dJ/dV) asymmetries arise due to an *internal* asymmetry of the DQD when reservoirs are coupled to the interacting region. Our use of

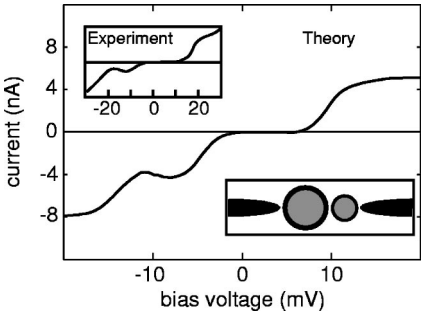

FIG. 1. A typical *J-V* characteristics calculated within the theory developed in this paper, further discussed in Sec. IV. The upper inset shows a typical experimental *J-V* result on the DQD reported in Ref. 10. The lower inset shows the geometry of the DQD system.

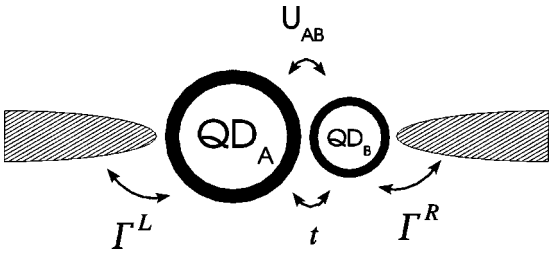

FIG. 2. Sketch of the double quantum dot system. The QDs interact via the interdot Coulomb repulsion U_{AB} and hopping t. The coupling strength between the DQD and the left/right contact is denoted by $\Gamma^{L/R}$.

many-body states rather than single particle states is motivated by the simple and uniform inclusion of intra- and interdot correlations. In the present formulation it is relevant to study the transitions between states in the DQD, rather than levels. Thus, it will be demonstrated that the probability amplitudes for the transitions between the states $|N-1,n\rangle$ and $|N,n\rangle$, where n is a state label of the N electron configuration of the DQD, are asymmetric with respect to the left and right contacts whenever the relative level spacing of the two QDs is finite. Moreover, the transition $|N,n\rangle\langle N-1,n|$ may couple stronger to, say, the left contact whereas $|N,n'\rangle\langle N-1,n|$, $n'\neq n$, could couple stronger to the right contact. In other words one may say that the states $|N,n\rangle$ and $|N,n'\rangle$ have their main weights on different QDs, although their corresponding wave functions are extended throughout the DQD. The local properties of the DQD are here studied in terms of many-body (Hubbard) operator nonequilibrium Green's-functions (GFs) beyond mean field theory, and it is found that the spectral weights for the transitions are dynamically (bias voltage dependent) redistributed as the bias voltage is varied. As we shall demonstrate, the internal asymmetry of the DQD results in a decreased probability amplitude at the resonance bias voltage for the corresponding transitions, which functions asymmetrically with respect to the bias voltage. The effects are seen even for DQDs with a symmetric *external* coupling to the left and right contacts.

As a result of the theoretical development in this paper we find very good agreement with recent experimental data on a DQD system constituted of two coupled carbon nanotubes.[10] However, before we go into the details of the theory we show in Fig. 1 a typical calculated *J-V* characteristics of the DQD system we consider in this paper. The upper inset in Fig. 1 displays an example of the experimental *J-V* result reported in Ref. 10. It should be noted in Fig. 1 that both the *J-V* asymmetry as well as the resonant peak are captured within the theoretical result. In the following sections we will describe the important features that have to be included in order to obtain such a result.

Despite the possible importance of the aforementioned sources for asymmetric *J-V* characteristics, e.g., impurities, unintentional charging effects, and asymmetric charge storage, we neglect such influences and consider the ideal situation, in order to illustrate the importance of the effects from strong electron correlations within the DQD. In most quantum devices there is more than one electron participating in the conductance through the interacting region. However, the source for the asymmetric *J-V* characteristics is present in any transition that adds/removes one electron to/from the interacting region. Thus, it is appropriate to consider only the case of single-electron tunneling through the system.

In this paper we disregard Kondo-like effects on the system, since such effects are of main importance for temperatures below the Kondo temperature,[21] which is not the case here. Second, possible (small) contributions from the Kondo effect cannot by themselves introduce the large degree of asymmetry often observed in experiments, since any Kondo resonance is suppressed by the application of a bias voltage.[22] Nevertheless, for low fields such contributions may slightly amplify the asymmetry introduced by the mechanism proposed in this paper.

The rest of this paper is organized as follows. In Sec. II we describe the model for the DQD which is followed by a derivation of the local properties of the DQD in Sec. III. We present numerical results of the *J-V* (dJ/dV) characteristics in Sec. IV and the paper is summarized and concluded in Sec. V.

II. MODELING THE DOUBLE QUANTUM DOT

Consider two QDs electrostatically coupled in series and connected to external contacts, see Fig. 2. In each of the QDs there is a large Coulomb repulsion $U_{A/B}$ and the QDs interact via the charging energy U_{AB} and the hopping t. In general, the interdot Coulomb energy $U_{AB}<U_{A/B}$, whereas the hopping $t\sim v_{k\sigma}$, where $v_{k\sigma}$, $k\in L,R$ is the hybridization between the states in the DQD and the states of the left (L) and the right (R) contact.

The energy of the DQD is here modeled by the following Hamiltonian

$$\mathcal{H}_{DQD}=\sum_{\sigma}\varepsilon_{A\sigma}d_{A\sigma}^{\dagger}d_{A\sigma}+U_{A}n_{A\uparrow}n_{A\downarrow}+\sum_{\sigma}\varepsilon_{B\sigma}d_{B\sigma}^{\dagger}d_{B\sigma}+U_{B}n_{B\uparrow}n_{B\downarrow}+U_{AB}(n_{A\uparrow}+n_{A\downarrow})(n_{B\uparrow}+n_{B\downarrow})+\sum_{\sigma}(t\,d_{A\sigma}^{\dagger}d_{B\sigma}+\text{H.c.}),\tag{1}$$

where $d_{A\sigma/B\sigma}^{\dagger}$ ($d_{A\sigma/B\sigma}$) creates (annihilates) an electron in $QD_{A/B}$ at the single-particle energy $\varepsilon_{A\sigma/B\sigma}$, whereas $n_{A\sigma}$

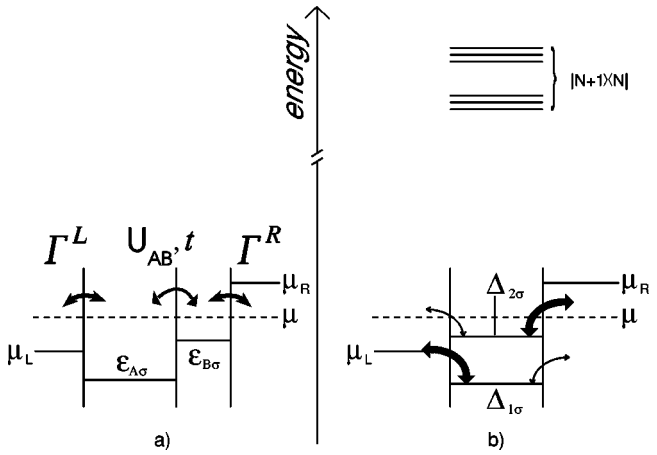

FIG. 3. (a) Sketch of the energy parameters of the serial DQD coupled to external contacts. In $QD_{A/B}$ the bare single-particle energy is $\varepsilon_{A\sigma/B\sigma}$ (for other parameters we refer to the text). (b) Schematic picture of the energies of the DQD system in the diagonal representation, where $\mu_{L/R}$ is the (quasi-) chemical potential of the left/right contact. The energy for a transition between the empty state and one-particle state $|\gamma_{n\sigma}\rangle$, $n=1,2$, is denoted by $\Delta_{n\sigma}$. The arrows illustrate the strengths of the transition probabilities between the one-particle states in the DQD and the contacts. In this configuration, the higher transitions, e.g., $|N+1\rangle\langle N|$ etc., lie outside the range of conduction.

$=d^{\dagger}_{A\sigma/A\sigma}(n_{B\sigma}=d^{\dagger}_{B\sigma/B\sigma})$ and σ denotes the spin. By the complexity of this model and knowing that the intra- and interdot Coulomb repulsions are the largest quantities of the system, it is preferable to rewrite it in terms of its many-body eigenstates, given in Ref. 23 for the case $U_B\to\infty$. The energies of the DQD are shown schematically in Fig. 3. The energy of the DQD can now be written in diagonal form, as follows:

$$\mathcal{H}_{\mathrm{DQD}}=\sum_p E_p h^p, \tag{2}$$

where $h^p\equiv X^{pp}$ and $X^{pq}\equiv|p\rangle\langle q|$ is a Hubbard operator[24,25] which describes the transition from the state $|q\rangle$ to $|p\rangle$. In Eq. (2), the index p runs over all possible states in the DQD described by Eq. (1). For bias voltages less than $U_{A/B}$ and the level separation of each of the QDs, it is sufficient to consider only transitions between the empty and singly occupied states $|0\rangle$ and $|\gamma_{n\sigma}\rangle$, $n=1,2$, respectively. Therefore, Eq. (2) reduces to a sum over $p\in\{0,\gamma_{1\sigma},\gamma_{2\sigma}\}$. It is important to note that in the experimental situation there may in the DQD be an unknown, large number of electrons. Since the conducting channels only involve one or few of the corresponding many-body states one can make a simplification and identify the empty state of our model with the $N-1$ state of the DQD. The exact eigenenergies for the one-particle many-body states are given by

$$E_{n\sigma}=\frac{\varepsilon_{A\sigma}+\varepsilon_{B\sigma}+(-1)^n\sqrt{(\varepsilon_{A\sigma}-\varepsilon_{B\sigma})^2+4t^2}}{2}, \tag{3}$$

for $n=1,2$, whereas the energy of the empty state is $E_0=0$.

TABLE I. Equilibrium properties of the DQD given the interdot Coulomb repulsion $U_{AB}=40$ meV and the hopping $t=0.75$ meV. The single-particle levels $\varepsilon_{A\sigma/B\sigma}$ are input parameters.

	(A)	(B)	(C)
$\varepsilon_{A\sigma}$ (meV)	−3.25	−2.5	−1.75
$\varepsilon_{B\sigma}$ (meV)	−1.75	−2.5	−3.25
$E_{1\sigma}$ (meV)	−3.56	−3.25	−3.56
$E_{2\sigma}$ (meV)	−1.44	−1.75	−1.44
$\lvert(a_\sigma)^{0\gamma_{1\sigma}}\rvert^2$	0.85	0.5	0.15
$\lvert(a_\sigma)^{0\gamma_{2\sigma}}\rvert^2$	0.15	0.5	0.85
$\lvert(b_\sigma)^{0\gamma_{1\sigma}}\rvert^2$	0.15	0.5	0.85
$\lvert(b_\sigma)^{0\gamma_{2\sigma}}\rvert^2$	0.85	0.5	0.15

The diagonal description of the DQD is convenient when the contacts are attached to the system. However, it is important to note that the transition matrix elements of the DQD in general are different for the transitions $|0\rangle\langle\gamma_{1\sigma}|$ and $|0\rangle\langle\gamma_{2\sigma}|$. These matrix elements are given by $(d_{A\sigma'})^{0\gamma_{n\sigma}}\equiv\langle 0|d_{A\sigma'}|\gamma_{n\sigma}\rangle=\delta_{\sigma\sigma'}u^{\sigma}_{n1}$ and $(d_{B\sigma'})^{0\gamma_{n\sigma}}\equiv\langle 0|d_{B\sigma'}|\gamma_{n\sigma}\rangle=\delta_{\sigma\sigma'}u^{\sigma}_{n2}$, where

$$u^{\sigma}_{n1}=\frac{E_{1\sigma}-B\sigma}{\sqrt{(E_{1\sigma}-\varepsilon_{B\sigma})^2+t^2}},$$

$$u^{\sigma}_{n2}=\frac{t}{\sqrt{(E_{1\sigma}-\varepsilon_{B\sigma})^2+t^2}}. \tag{4}$$

Hence, $|(d_{A\sigma'})^{0\gamma_{1\sigma}}|^2\neq|(d_{A\sigma'})^{0\gamma_{2\sigma}}|^2$ and $|(d_{B\sigma'})^{0\gamma_{1\sigma}}|^2\neq|(d_{B\sigma'})^{0\gamma_{2\sigma}}|^2$ whenever $\varepsilon_{A\sigma}\neq\varepsilon_{B\sigma}$, as can be seen in Table I and Fig. 4, where the equilibrium properties of the DQD and the transition matrix elements are listed and plotted, respectively. This situation holds true for most realistic systems since the sizes of the two QDs in general are different. The difference of the transition matrix elements influences the current through the system. Furthermore, through the transition matrix elements one can control whether an electron escapes/enters the DQD to/from the left or the right contact.

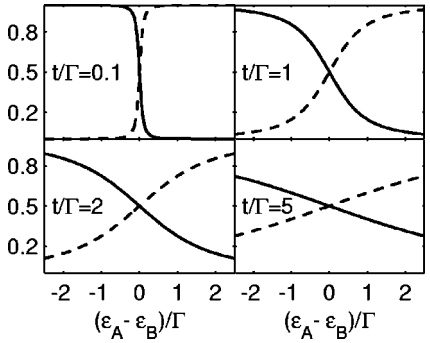

FIG. 4. The transition matrix elements $|(d_{A\sigma})^{0\gamma_{1\sigma}}|^2=|(d_{B\sigma})^{0\gamma_{2\sigma}}|^2$ (solid) and $|(d_{A\sigma})^{0\gamma_{2\sigma}}|^2=|(d_{B\sigma})^{0\gamma_{1\sigma}}|^2$ (dashed) as functions of the relative level spacing $(\varepsilon_A-\varepsilon_B)/\Gamma$ for various hopping strengths t/Γ.

The plots in Fig. 4 illustrate the dependence of the transition matrix elements $|(d_{A\sigma})^0\gamma_{1\sigma}|^2=|(d_{B\sigma})^0\gamma_{2\sigma}|^2$ (solid) and $|(d_{A\sigma})^0\gamma_{2\sigma}|^2=|(d_{B\sigma})^0\gamma_{1\sigma}|^2$ (dashed) on the relative level spacing $(\varepsilon_A-\varepsilon_B)/\Gamma$ for various hopping strengths t/Γ. As is seen, the transition matrix elements are equal for a vanishing relative level spacing, for all hopping strengths. This is understood, since then $E_{n\sigma}-\varepsilon_{B\sigma}=(-1)^2t$ which gives $|u^\sigma_{n1}|^2=t^2/(2t^2)=1/2=|u^\sigma_{n2}|^2$. This is expected since the states in the two QDs then are in resonance. Thus, this means that the two one-particle states are equally distributed throughout the DQD.

For finite relative level spacing ($\varepsilon_{AB}\equiv\varepsilon_{A\sigma}-\varepsilon_{B\sigma}\neq 0$), though, one of the matrix elements tends to approach 1 and the other to 0, as $2t/\varepsilon_{AB}\to 0$. In this situation, $E_{n\sigma}-\varepsilon_{B\sigma}\approx \mathrm{sign}(\varepsilon_{AB})+(-1)^n$, which leads to that

$$|u^\sigma_{n1}|^2\approx\frac{[\mathrm{sgn}(\varepsilon_{AB})+(-1)^n]^2}{[\mathrm{sgn}(\varepsilon_{AB})+(-1)^n]^2+(2t/\varepsilon_{AB})^2},$$

$$|u^\sigma_{n2}|^2\approx\frac{(2t/\varepsilon_{AB})^2}{[\mathrm{sgn}(\varepsilon_{AB})+(-1)^n]^2+(2t/\varepsilon_{AB})^2}.$$

For definiteness suppose that $\varepsilon_{AB}<0$. Then, $|u^\sigma_{11}|^2=4/(4+(2t/\varepsilon_{AB})^2)\to 1$ as $|\varepsilon_{AB}/(2t)|\to\infty$, whereas $|u^\sigma_{21}|^2\to 0$, as is seen in the upper left panel of Fig. 4. Similarly it is found that $|u^\sigma_{12}|^2\to 0$ and $|u^\sigma_{22}|^2\to 1$. Physically this means that the state $|\gamma_{1\sigma}\rangle$ has a larger weight on QD_A than on QD_B while $|\gamma_{2\sigma}\rangle$ has a larger weight on QD_B. The case when $\varepsilon_{AB}>0$ is found in the same way, showing that $|u^\sigma_{11}|^2,|u^\sigma_{22}|^2\to 0$ whereas $|u^\sigma_{21}|^2,|u^\sigma_{12}|^2\to 1$.

In the opposite limit, e.g., $\varepsilon_{AB}/(2t)\to 0$, we have that $E_{n\sigma}-\varepsilon_{B\sigma}\approx t[(-1)^n+\varepsilon_{AB}/(2t)]$ leading to

$$|u^\sigma_{n1}|^2\approx\frac{[(-1)^n+\varepsilon_{AB}/(2t)]^2}{1+[(-1)^n+\varepsilon_{AB}/(2t)]^2}\to\frac{1}{2},$$

$$|u^\sigma_{n2}|^2\approx\frac{1}{1+[(-1)^n+\varepsilon_{AB}/(2t)]^2}\to\frac{1}{2},$$

as is indicated in Fig. 4 for increasing t/Γ. Hence, the one-particle states become more and more equally distributed throughout the DQD for increasing hopping strengths, which is expected since a large hopping, in general, tends to delocalize the states in a system.

III. SCATTERING BETWEEN THE STATES

In this section, the nonequilibrium Green's-function (GF) of the DQD will be derived and discussed with respect to the scattering between the states in the DQD. The whole system, constituted by the DQD and the contacts is modeled by

$$\mathcal{H}=\sum_{k\sigma\in L,R}\varepsilon_{k\sigma}c^\dagger_{k\sigma}c_{k\sigma}+\mathcal{H}_{\mathrm{DQD}}+\sum_{kn\sigma}(v_{kn\sigma}c^\dagger_{k\sigma}X^{0\gamma_{n\sigma}}+\mathrm{H.c.}),\tag{5}$$

where $v_{kn\sigma}=v_{k\sigma}(d_\sigma)^{0\gamma_{n\sigma}}$ and $d_\sigma=d_{A\sigma}$ or $d_\sigma=d_{B\sigma}$ depending on whether an electron escapes the DQD to the left or the right contact. The current through this system, as a function of the applied bias voltage, is expressed by the formula[26–28]

$$J=-\frac{e}{2h}\mathrm{Im}\sum_{n\sigma}\int\{[\Gamma^L_{n\sigma}(\omega)-\Gamma^R_{n\sigma}(\omega)]G^<_{n\sigma}(\omega)+[f_L(\omega)\Gamma^L_{n\sigma}(\omega)-f_R(\omega)\Gamma^R_{n\sigma}(\omega)][G^r_{n\sigma}(\omega)-G^a_{n\sigma}(\omega)]\}d\omega,\tag{6}$$

where $\Gamma^{L/R}_{n\sigma}(\omega)=2\pi\Sigma_{k\in L/R}|v_{kn\sigma}|^2\delta(\omega-\varepsilon_{k\sigma})$ is the coupling strength between the nth DQD state and the left/right contact, whereas $f_{\mathrm{L/R}}(\omega)=f(\omega-\mu_{\mathrm{L/R}})$ is the Fermi distribution function and $\mu_{\mathrm{L/R}}$ is the (quasi-) chemical potential of the left/right contact. In Eq. (6), the Fourier transform of the lesser, retarded, and advanced DQD GF appear, defined by

$$G_{n\sigma}(t,t')=(-i)\langle\mathrm{T}X^{0\gamma_{n\sigma}}(t)X^{\gamma_{n\sigma}0}(t')\rangle_U=(-i)\frac{\langle\mathrm{T}SX^{0\gamma_{n\sigma}}(t)X^{\gamma_{n\sigma}0}(t')\rangle}{\langle\mathrm{T}S\rangle},\tag{7}$$

where the action $S=\exp[-i\int_{t_0}^{t_0-i\beta}\mathcal{H}'(t)dt]$ and the disturbance potential

$$\mathcal{H}'(t)=U_0(t)h^0+\sum_{n\sigma}\left(U_{n\sigma}(t)h^{\gamma_{n\sigma}}+U_{n\sigma\bar\sigma}(t)Z^{\gamma_{n\sigma}\gamma_{n\bar\sigma}}+\sum_{\sigma',m\neq n}U_{nm\sigma\sigma'}(t)Z^{\gamma_{n\sigma}\gamma_{m\sigma'}}\right),\tag{8}$$

in which $Z^{\gamma_{n\sigma}\gamma_{m\sigma'}}=|\gamma_{n\sigma}\rangle\langle\gamma_{m\sigma'}|$ denotes a transition between states such that the total spin of the DQD is changed by an integer. By means of functional derivatives with respect to the source fields $U_\xi(t)$ introduced in Eq. (8), a diagrammatic expansion of the DQD GF is generated in terms of even powers of the hybridization matrix element $v_{kn\sigma}$. Physical quantities are extracted from $G_{n\sigma}(t,t')$ in the limit $U_\xi(t)\to 0$. For further details on the definition of the DQD GF, see Refs. 28–30.

The equation of motion of the $G_{n\sigma}(t,t')$ is given by

$$\left(i\frac{\partial}{\partial t}-\Delta^0_{n\sigma}-\Delta U_{n\sigma}(t)\right)G_{n\sigma}(t,t')-U_{n\sigma\bar\sigma}(t)G_{n\bar\sigma\sigma}(t,t')-\sum_{\sigma',m\neq n}U_{nm\sigma\sigma'}G_{m\sigma' n\sigma}(t,t')=\delta(t-t')P_{n\sigma}(t)+\sum_{m\sigma'}[P_{n\sigma m\sigma'}(t^+)+R_{n\sigma m\sigma'}(t^+)]\times\int_{t_0}^{t_0-i\beta}V_{m\sigma'}(t,t_1)G_{m\sigma' n\sigma}(t_1,t')dt_1.\tag{9}$$

Here, $G_{n\sigma m\sigma'}(t,t)\equiv(-i)\langle\mathrm{T}X^{0\gamma_{n\sigma}}(t)X^{\gamma_{m\sigma'}0}(t')\rangle_U$ whereas $G_{n\sigma\bar\sigma}(t,t')\equiv G_{n\sigma n\bar\sigma}(t,t')$ where $\bar\sigma$ denotes the opposite spin projection of σ. Moreover, $P_{n\sigma m\sigma'}(t)\equiv\langle\mathrm{T}\{X^{0\gamma_{n\sigma}},X^{\gamma_{m\sigma'}0}\}(t)\rangle$ is the *end-factor* of the DQD GF where $P_{n\sigma}(t)\equiv P_{n\sigma n\sigma}(t)$, whereas $R_{n\sigma m\sigma'}(t)\equiv i[\delta_{\sigma\sigma'}\delta_{nm}\delta/\delta U_0(t)+\delta/\delta U_{m\sigma' n\sigma}(t)]$ is the functional differential operator (note the order of the indices in the second term of this operator). Finally, the propagator $V_{n\sigma}(t,t')=\Sigma_k|v_{kn\sigma}|^2g_{k\sigma}(t,t')$ where $g_{k\sigma}(t,t')$ is the GF for the electrons in the contacts, satisfying the equation of motion $(i\partial/\partial t-\varepsilon_{k\sigma})g_{k\sigma}(t,t')=\delta(t-t')$.

In the present formulation, the DQD GF is constituted of the product $G_{n\sigma n'\sigma'}(t,t')=\Sigma_{m\sigma_1}D_{n\sigma m\sigma_1}(t,t')P_{m\sigma_1 n'\sigma'}(t')$, where $D_{n\sigma m\sigma_1}(t,t')$ is the *locator* which contains the pole and self-energy, whereas the end-factor $P_{m\sigma_1 n'\sigma}(t')$ carries the spectral weight of the DQD GF. This means that any functional differentiation of the DQD GF should be applied to both the locator $D_{n\sigma m\sigma_1}(t,t')$ as well as the end-factor $P_{m\sigma_1 n'\sigma'}(t')$. Hence,

$$\delta G_{n\sigma n'\sigma'}(t,t') = \sum_{m\sigma_1} \{[\delta D_{n\sigma m\sigma_1}(t,t')]P_{m\sigma_1 n'\sigma'}(t') + D_{n\sigma m\sigma_1}(t,t')[\delta P_{m\sigma_1 n'\sigma'}(t')]\}.$$

For the functional differentiation of the locator, the matrix property $\mathbf{DD}^{-1}=\mathbf{I}=\mathbf{D}^{-1}\mathbf{D}$ is employed, thus giving

$$\begin{aligned}\delta G_{n\sigma n'\sigma'}(t,t') = &\sum_{m\sigma_1} D_{n\sigma m\sigma_1}(t,t')[\delta P_{m\sigma_1 n'\sigma'}(t')] \\ &- \sum_{mm'm''\sigma_1\sigma_1\sigma_3}\int_{t_0}^{t_0-i\beta} D_{n\sigma m\sigma_1}(t,t_1) \\ &\times[\delta D^{-1}_{m\sigma_1 m'\sigma_2}(t_2,t_3)] \\ &\times D_{m'\sigma_2 m''\sigma_3}(t_3,t')P_{m''\sigma_3 n'\sigma'}(t')dt_1\,dt_2\,dt_3.\end{aligned}$$

In the limit of zero source fields $U_\xi(t)\to 0$, all components of the DQD Green's-function matrix that do not conserve either spin or orbital moments vanish, although functional derivatives thereof may be finite. Scattering between the one-particle states $|\gamma_{1\sigma}\rangle$ and $|\gamma_{2\sigma'}\rangle$ are included in the first order correction with respect to the number of functional derivatives applied both to the locator and the end-factor of the DQD GF. Keeping these observations in mind, one finds that the resulting expression for $R_{n\sigma m\sigma'}(t^+)G_{m\sigma' n\sigma}(t_1,t')$ in Eq. (9) can be written as

$$\begin{aligned}&\sum_{m\sigma'} R_{n\sigma m\sigma'}(t^+)\int_{t_0}^{t_0-i\beta} V_{m\sigma'}(t,t_1)G_{m\sigma' n\sigma}(t_1,t')dt_1 \\ &\quad = i\sum_{m\sigma'}(1-\delta_{mn}\delta_{\sigma\sigma'}) \\ &\qquad \times\left(K_{m\sigma' n\sigma}(t^+,t')\int_{t_0}^{t_0-i\beta} V_{m\sigma'}(t,t_1)D_{m\sigma'}(t_1,t')dt_1\right. \\ &\qquad \left. + \int_{t_0}^{t_0-i\beta} V_{m\sigma'}(t,t_1)D_{m\sigma'}(t_1,t^+)dt_1\, G_{n\sigma}(t^+,t')\right). \quad (10)\end{aligned}$$

Here, $K_{m\sigma' n\sigma}(t,t')\equiv(-i)\langle \mathrm{T}Z^{\gamma_{m\sigma'}\gamma_{n\sigma}}(t)Z^{\gamma_{n\sigma}\gamma_{m\sigma'}}(t')\rangle_U$ is the GF for the Bose-like scattering processes between the different one-particle states, which satisfies the equation of motion $(i\partial/\partial t-\Delta_{n\sigma m\sigma'})K_{m\sigma' n\sigma}(t,t')=\delta(t-t')[P_{m\sigma'}(t)-P_{n\sigma}(t)]$, $\Delta_{n\sigma m\sigma'}\equiv\Delta_{n\sigma}-\Delta_{m\sigma'}$, where $\Delta_{n\sigma}$ is the dressed transition energy for the transition $|0\rangle\to|\gamma_{n\sigma}\rangle$, defined below.

The first term on the right-hand side of Eq. (10), plays an essential role in the understanding of the scattering effects that influence the transport through the system. In particular, this term is a key part for the explanation of the current-voltage (J-V) asymmetries as well as the asymmetric negative differential resistance, as will be discussed below. The second term of Eq. (10) gives a contribution to the transition energy due to kinematic interactions between the one-particle states induced by the presence of the conduction electrons in the contacts. This is a characteristic feature for complexes of systems with interactions between localized and delocalized electrons.

Now, identify the dressed transition energy $\Delta_{n\sigma}(t)$ by

$$\Delta_{n\sigma}(t) = \Delta^0_{n\sigma} + i\sum_{m\sigma'}(1-\delta_{nm}\delta_{\sigma\sigma'}) \times\int_{t_0}^{t_0-i\beta} V_{m\sigma'}(t,t_1)D_{m\sigma'}(t_1,t^+)dt_1 \quad (11)$$

and the dressed end-factor $\mathbb{P}_{n\sigma}(t,t')$ by

$$\mathbb{P}_{n\sigma}(t,t') = \delta(t-t')P_{n\sigma}(t) + i\sum_{m\sigma'} K_{m\sigma' n\sigma}(t^+,t') \times\int_{t_0}^{t_0-i\beta} V_{m\sigma'}(t,t_1)D_{m\sigma'}(t_1,t')dt_1. \quad (12)$$

Notice that the propagator $K_{m\sigma' n\sigma}(t,t')$ is zero when $m=n$ and $\sigma'=\sigma$. Thus, it is not necessary to explicitly insert the factor $(1-\delta_{nm}\delta_{\sigma'\sigma})$ into the expression given in Eq. (12), as it is done in Eq. (11). However, in both the dressed transition energy and end-factor the contribution at $m=n,\sigma'=\sigma$ has to vanish in order to exclude self-interactions within the system. In the given notation, the DQD GF can be written as [in the limit $U_\xi(t)\to 0$]

$$\begin{aligned}&\left(i\frac{\partial}{\partial t}-\Delta_{n\sigma}\right)G_{n\sigma}(t,t') \\ &\quad = \mathbb{P}_{n\sigma}(t,t') + \int_{t_0}^{t_0-i\beta}\mathbb{P}_{n\sigma}(t,t_1)V_{n\sigma}(t_1,t_2)G_{n\sigma}(t_2,t')dt_1\,dt_2.\end{aligned} \quad (13)$$

The DQD GF in Eq. (13) with the correction given in Eq. (10) will henceforth be referred to as the *full loop approximation*, whereas the approximation with the bare end-factor and with the dressed transition energies is the so-called *loop correction*.[29,28] The approximation where both the end-factors and transition energies being bare is the well-known Hubbard I approximation (HIA).[24,25,30,31] As is known, the HIA is a mean field approximation which is also the case for the loop correction in the sense that the spectral weight is energy independent. However, it should be noted that these quantities may vary under influence of external fields. We emphasize though, that the loop correction contains a renormalization of the transition energies that is strongly dynamically dependent on the properties in the conduction bands and the hybridization between the localized and delocalized states, see Refs. 28, 29, and 32. Thus, this approximation goes far beyond any standard mean field theory. In the full loop approximation, the dressing of the end-factor introduces an energy dependence of the spectral weight, which will be further discussed in the following section. Moreover, in this approximation also the spectral weight and the imaginary part of the self-energy become explicitly dependent on external field, e.g., the bias voltage in the present case.

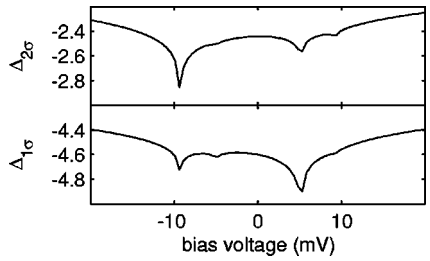

FIG. 5. Dressed transition energies as functions of the bias voltage for case (A) in Table I with $\Gamma^{L/R}=0.375$ meV at $T=5$ K.

A. Basic properties of the DQD GF

In this paper the transport through the DQD will be analyzed in the stationary regime, which makes it preferable to Fourier transform the equations into energy variables, that is

$$(i\omega-\Delta_{n\sigma})G_{n\sigma}(i\omega)=\mathbb{P}_{n\sigma}(i\omega)+\mathbb{P}_{n\sigma}(i\omega)V_{n\sigma}(i\omega)G_{n\sigma}(i\omega). \tag{14}$$

In this regime, the dressed transition energy becomes

$$\Delta_{n\sigma}=\Delta^0_{n\sigma}+\sum_{m\sigma'}(1-\delta_{nm}\delta_{\sigma\sigma'})\sum_{k\in L,R}\frac{|v_{km\sigma'}|^2}{2\pi}\times\int[-2\ \mathrm{Im}\ D^r_{m\sigma'}(\omega)]\frac{f(\varepsilon_{k\sigma'})-f(\omega)}{\varepsilon_{k\sigma'}-\omega}d\omega, \tag{15}$$

where $D^r_{m\sigma'}(\omega)$ is the retarded form of the dressed DQD locator for the transition $|0\rangle\rightarrow|\gamma_{m\sigma'}\rangle$. The second term of Eq. (15) gives a shift of the energy of the transition $|0\rangle\rightarrow|\gamma_{m\sigma}\rangle$ from interactions between the different one-particle states and the conduction electrons in the contacts. It is clear from this equation that contributions from self-interactions are excluded, since it is the strong Coulomb repulsion acting between the localized states in the DQD that causes the shift, however, induced by the presence of the conduction electrons in the contacts. It is also clear that the shift increases as the (quasi-) chemical potential in one (or both) of the contacts approaches any of the transition energies involved in the sum on the right-hand side of Eq. (15). This is illustrated in Fig. 5 where we show the dressed transition energies as functions of the bias voltage for the case (A) in Table I. We note that the cases listed in Table I are reasonable for sizes of the QDs $\lesssim 10-100$ nanometers each. It may be seen from the figure that sharp dips in $\Delta_{n\sigma}$ are found at specific bias voltages. If the couplings to the left and the right contact are asymmetric, that is, if the hybridization between the localized state in the DQD and the states in the left contact is different from that to the right contact, then the shift of the transition energies becomes different when the bias voltages is applied in forward direction compared to the reverse biased system. In Fig. 5 the couplings $\Gamma^L=\Gamma^R[\Gamma^\alpha=2\pi\Sigma_{k\in\alpha}|v_{k\sigma}|^2\delta(\omega-\varepsilon_{k\sigma}),\alpha=L,R]$, however, the couplings of each DQD transition become asymmetric with respect to the left and right contacts, i.e., $\Gamma^L_{n\sigma}\neq\Gamma^R_{n\sigma}$, due to the asymmetry of the transitions $|0\rangle\langle\gamma_{n\sigma}|$ inside the DQD. It should be emphasized that the result given in Eq. (15) also holds for the nonequilibrium situation since the dressed transition energy, Eq. (11), only depends on one time variable.

The corresponding dressed end-factor can be written as

$$\mathbb{P}_{n\sigma}(i\omega)=\mathbb{P}_{n\sigma}-\sum_{m\sigma'}\frac{P_{m\sigma'}-P_{n\sigma}}{2\pi}\times\int[-2\ \mathrm{Im}\ D^r_{m\sigma'}(\omega')]\sum_{k\in L,R}\frac{|v_{km\sigma'}|^2}{\varepsilon_{k\sigma'}-\omega'}\times\left(\frac{f(\varepsilon_{k\sigma'})-[n_B(\Delta_{n\sigma m\sigma'})+1]}{i\omega-\Delta_{n\sigma m\sigma'}-\varepsilon_{k\sigma'}}-\frac{f(\omega')-[n_B(\Delta_{n\sigma m\sigma'})+1]}{i\omega-\Delta_{n\sigma m\sigma'}-\omega'}\right)d\omega', \tag{16}$$

where $n_B(x)$ is the Bose function. The expression for the dressed end-factor given in Eq. (16) applies to nonequilibrium, however, it is inconvenient to use in such situations. The reason is that the chemical potential of the DQD is not known in the nonequilibrium case, whereas in equilibrium it is reasonable to introduce a common chemical potential for the system which equals the chemical potentials of the contacts.

The expression in Eq. (16) can be used to understand the basic mechanisms for the scattering between the one-particle states. First of all it should be noticed that any contribution in the sum over the states $|\gamma_{m\sigma'}\rangle$ vanishes whenever $P_{m\sigma'}=P_{n\sigma}$, that is, whenever the spectral weights of the transitions $|0\rangle\rightarrow|\gamma_{n\sigma}\rangle$ and $|0\rangle\rightarrow|\gamma_{m\sigma'}\rangle$ are equal. Second, the leading contribution from the dressing of the end-factor, the first term of Eq. (16), has an imaginary part which is peaked around $\Delta_{n\sigma}$. To illustrate this with a simple model, we put $-2\ \mathrm{Im}\ D^r_{m\sigma'}(\omega')=2\pi\delta(\omega'-\Delta_{m\sigma'})$, assume k-independent hybridization matrix elements, $v_{k\sigma}\rightarrow v_\sigma$, and wide and flat conduction bands in the contacts. These simplifications lead to the retarded end-factor

$$\mathbb{P}^r_{n\sigma}(\omega)=P_{n\sigma}-\sum_{m\sigma'}\frac{P_{m\sigma'}-P_{n\sigma}}{\omega-\Delta_{n\sigma}}\sum_{\alpha=L,R}\Gamma^\alpha_{m\sigma'}\times\left(\log\left|\frac{\mu_\alpha-\Delta_{m\sigma'}}{\omega-\Delta_{n\sigma m\sigma'}-\mu_\alpha}\right|-\frac{i}{2}f_\alpha(\omega-\Delta_{n\sigma m\sigma'})\right).$$

The real part of this expression appears to be diverging for bias voltages such that $\mu_\alpha\approx\Delta_{m\sigma}$. However, due to the finite width of the dressed locator $D^r_{m\sigma'}(\omega')$, used in the calculations for the current discussed in Sec. IV, its contribution to the dressing is less important. The physical effect from the dressing of the end-factor is an increased or decreased spectral weight for the corresponding GF, depending on the sign of the difference $P_{m\sigma'}-P_{n\sigma}$. Hence, the ability for an electron to tunnel through the DQD via the transition $|\gamma_{n\sigma}\rangle\langle 0|$ is highly affected by the scattering between the one-particle states. It should be emphasized, however, that this is a dynamical process which strongly depends on the bias voltage and, in addition, on the strength of the couplings to the left and the right contacts. We discuss this in more detail below.

B. Nonequilibrium equations

The correct nonequilibrium expressions for the DQD GF, hence also for the end-factor, are found by applying the Langreth rules for analytical continuation.[33] Thus, the lesser DQD GF becomes

$$G^<_{n\sigma}(\omega) = G^r_{n\sigma}(\omega)V^<_{n\sigma}(\omega)G^a_{n\sigma}(\omega) + D^r_{n\sigma}(\omega)\mathbb{P}^<_{n\sigma}(\omega) \times[1 + V^a_{n\sigma}(\omega)G^a_{n\sigma}(\omega)], \quad (17)$$

where the retarded/advanced DQD GF is given by

$$G^{r/a}_{n\sigma}(\omega) = \frac{\mathbb{P}^{r/a}_{n\sigma}(\omega)}{\omega - \Delta_{n\sigma} - \mathbb{P}^{r/a}_{n\sigma}(\omega)V^{r/a}_{n\sigma}(\omega)}. \quad (18)$$

Here, the retarded/advanced interaction operator $V^{r/a}_{n\sigma}(\omega) = \Lambda_{n\sigma}(\omega) \mp i\Gamma_{n\sigma}(\omega)/2$, whereas its lesser counterpart is given by $V^<_{n\sigma}(\omega) = i[f_L(\omega)\Gamma^L_{n\sigma}(\omega) + f_R(\omega)\Gamma^R_{n\sigma}(\omega)]$.

By inspection of Eq. (12) one finds that the lesser form of the dressed end-factor $\mathbb{P}_{n\sigma}(i\omega)$ is given by

$$\mathbb{P}^<_{n\sigma}(\omega) = \frac{i}{2\pi}\sum_{m\sigma'}\int K^<_{m\sigma' n\sigma}(\omega-\varepsilon)[V^r_{m\sigma'}(\varepsilon)D^<_{m\sigma'}(\varepsilon) + V^<_{m\sigma'}(\varepsilon)D^a_{m\sigma'}(\varepsilon)]d\varepsilon, \quad (19)$$

whereas the retarded/advanced form of the dressed end-factor becomes

$$\mathbb{P}^{r/a}_{n\sigma}(\omega) = P_{n\sigma} + \frac{i}{2\pi}\sum_{m\sigma'}\int (K^{r/a}_{m\sigma' n\sigma}(\omega-\varepsilon) \times [V^r_{m\sigma'}(\varepsilon)D^<_{m\sigma'}(\varepsilon) + V^<_{m\sigma'}(\varepsilon)D^a_{m\sigma'}(\varepsilon)] + [K^<_{m\sigma' n\sigma}(\omega-\varepsilon) + K^{r/a}_{m\sigma' n\sigma}(\omega-\varepsilon)] \times V^{r/a}_{m\sigma'}(\varepsilon)D^{r/a}_{m\sigma'}(\varepsilon))d\varepsilon. \quad (20)$$

Here, $K^<_{m\sigma' n\sigma}(\omega) = -i2\pi(P_{m\sigma'} - P_{n\sigma})n_B(\Delta_{n\sigma m\sigma'})\delta(\omega - \Delta_{n\sigma m\sigma'})$ whereas $K^{r/a}_{m\sigma' n\sigma}(\omega) = (P_{m\sigma'} - P_{n\sigma})/(\omega - \Delta_{n\sigma m\sigma'} \pm i\delta)$. Finally, the retarded/advanced and lesser forms of the dressed locator are given by

$$D^{r/a}_{n\sigma}(\omega) = \frac{1}{\omega - \Delta_{n\sigma} - \mathbb{P}^{r/a}_{n\sigma}(\omega)V^{r/a}_{n\sigma}(\omega)}$$

and

$$D^<_{n\sigma}(\omega) = D^r_{n\sigma}(\omega)[\mathbb{P}^r_{n\sigma}(\omega)V^<_{n\sigma}(\omega) + \mathbb{P}^<_{n\sigma}(\omega)V^a_{n\sigma}(\omega)]D^a_{n\sigma}(\omega),$$

respectively.

It is clear that the retarded/advanced and lesser counterparts of the dressed end-factor are necessary in order to calculate the corresponding forms of the DQD GF, cf. Eqs. (17) and (18). However, these expressions are also needed to find the nonequilibrium population numbers for the transitions $|\gamma_{n\sigma}\rangle\langle 0|$. The average of these population numbers are found from the identity

$$N_{n\sigma} = \frac{1}{2\pi}\mathrm{Im}\int G^<_{n\sigma}(\omega)d\omega \quad (21)$$

and the boundary condition $1 = N_0 + \Sigma_{n\sigma}N_{n\sigma}$.

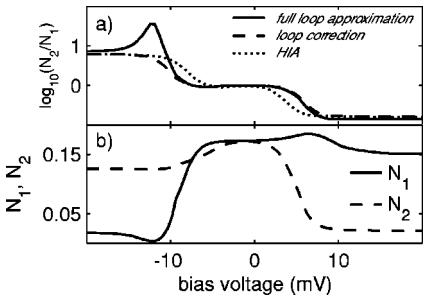

FIG. 6. Dressed population numbers $N_n = \Sigma_\sigma N_{n\sigma}$, $n = 1,2$, as functions of the bias voltage for case (A) in Table I.

The plots in Fig. 6(b) display the total population numbers $N_n = \Sigma_\sigma N_{n\sigma}$, $n = 1,2$, for the one-particle states as functions of the bias voltage for the parameters used for case (A), given in Table I. The population numbers N_n, are almost equal in the region around equilibrium. However, it may be seen from Fig. 6 that as the bias voltage is increased in the forward direction ($\mu_L - \mu_R > 0$), the population of $|\gamma_{2\sigma}\rangle\langle\gamma_{2\sigma}|$ decreases whereas the population of $|\gamma_{1\sigma}\rangle\langle\gamma_{1\sigma}|$ remains more or less constant. This behavior reflects the difference of the coupling strengths for the two transitions $|0\rangle\langle\gamma_{n\sigma}|$, $n = 1,2$. The first transition ($n = 1$) couples weaker to the right contact than the second ($n = 2$) and, hence prohibits electrons to flow through the DQD via this transition. Therefore, the population of this transition remains constant around its maximum value, for a large range of forward bias voltages. For backward bias voltages ($\mu_L - \mu_R > 0$), the case is quite the opposite, since then the first transition couples stronger to the left contact than the second (see Fig. 6). Hence a larger amount of electrons can flow through the DQD via the first transition and, thus, the population decreases very rapidly as this transition becomes resonant.

However, there is a hump and a dip in Fig. 6 for N_1 around 9 and −11 mV, respectively, both which are caused by the dressing of the end-factor. This fact is emphasized in Fig. 6(a) which shows a comparison of the two mean field approximations, HIA (dotted) and with the loop correction (dashed), and the full loop approximation (solid). The figure illustrates a logarithmic plot of the quotient N_2/N_1 as a function of the bias voltage in the three approximation schemes. The dynamical (bias voltage dependent) effects from the dressed end-factor tend to modify the populations of the transitions for bias voltages around $\Delta_{n\sigma}$, discussed in the previous section. This modification leads to a further decrease of N_1 for bias voltages around −11 mV since the difference $P_{2\sigma} - P_{1\sigma} > 0$, cf. Eq. (16), whereas for bias voltages around 9 mV the difference $P_{2\sigma} - P_{1\sigma} < 0$ which leads to the hump in N_1. In mean field theory, the electrons flow through the DQD directly via the transitions $|\gamma_{n\sigma}\rangle\langle 0|$. This is expected since the transversal transitions $|\gamma_{1\sigma}\rangle\langle\gamma_{2\sigma}|$, and $|\gamma_{2\sigma}\rangle\langle\gamma_{1\sigma}|$, are not included into the Hamiltonian, Eq. (5). However, the dynamical (voltage dependent) behavior of the dressed end-factor, which includes effects from these transitions, ruins this scenario since it tends to decrease (increase) the population number N_1 around −11 mV (9 mV). Hence, the correction diagram from scattering between the one-particle states in the DQD tends to prevent electrons in the contacts to

tunnel through the DQD via the transition $|\gamma_{1\sigma}\rangle\langle 0|$.

As a result of this dynamical redistribution of the spectral weights, it is expected that the current through the DQD for bias voltages around −11 mV (9 mV) in the full loop approximation will be less than the corresponding currents given within the mean field approximations. Nevertheless, since both transitions from the empty state to the one-particle states, $|\gamma_{n\sigma}\rangle\langle 0|$, $n=1,2$, are resonant around −11 mV whereas only $|\gamma_{2\sigma}\rangle\langle 0|$ is resonant around 9 mV, it is also expected that the influence of this dynamical re-distribution on the resulting current should be larger in the former case than in the latter. This will be further discussed in the following section. The asymmetry of the positions of the hump and the dip with respect to the forward and backward biased system is related to the asymmetric renormalization of the transition energies, as can be seen in Fig. 5.

IV. CURRENT-VOLTAGE CHARACTERISTICS

In this section we will analyze the calculated current under various circumstances. The important parameters in the present context are the level separation $\varepsilon_A-\varepsilon_B$, that is the relative positions of the levels in $\mathrm{QD}_{A/B}$, and the hopping strength between the two QDs. These should be compared with the coupling strengths $\Gamma^{\mathrm{L/R}}$ between the DQD and left/right reservoir. The parameters for Coulomb repulsion internally and between the QD are irrelevant as long as we restrict the discussion to bias voltages such that only the transitions between the empty state and the one-particle states contribute to the conductance. For bias voltages such that the states with more than one particle contribute to the conduction, a more complete analysis has to be done in addition to the one in the present case. However, we expect that similar effects, as the one discussed here, related to the dressed end-factors, will be present also in this case. Hence, the resulting *J-V* asymmetries and possible negative differential conductance will be amplified when transitions to states with more than one electron are included.

In the stationary regime, the nonequilibrium properties of the DQD are found from self-consistent calculations of Eqs. (15), (17), (18), and (21) for each value of the bias voltage $V_{\mathrm{bias}}=(\mu_L-\mu_R)/e$. The bias voltage is inserted into the dressed transition energy, Eq. (15) and the lesser interaction propagator $V^{<}_{n\sigma}(\omega)$, and thereafter in the DQD GF. In this fashion, the voltage dependence of the dressed end-factor (and transition energies) is taken into account and, hence, the voltage dependence of the population numbers of the transitions between the empty state and the one-particle states. Thus, the dynamical behavior of the spectral weights (end-factors) will be included when the bias voltage is varied and the condition for an increased scattering between the one-particle states becomes fulfilled, leading to the *J-V* asymmetries and negative differential resistance to be discussed in the following.

The current in this paper is calculated by means of the expression given in Eq. (6) where the DQD GF is given within the full loop approximation (dressed transition energies and end-factors), the loop correction (dressed transition energies and bare end-factors) and the HIA (bare transition energies and end-factors). The corresponding differential conductance (dJ/dV) is computed as a numerical derivative of the current with respect to the bias voltage. The numerical derivative has been chosen since an accurate analytical expression is available only in the low bias regime, e.g., in linear response. The reason for this is that both the transition energies and end-factors, hence the DQD GFs and their self-energies, are bias voltage dependent. Although some properties of the *J-V* asymmetries are seen already in the linear response theory, the more interesting nonlinear features of the current through the DQD comes about at higher fields. Moreover, the negative differential conductance behavior will not be seen in a linear response theory and therefore we disregard any analysis within this regime.

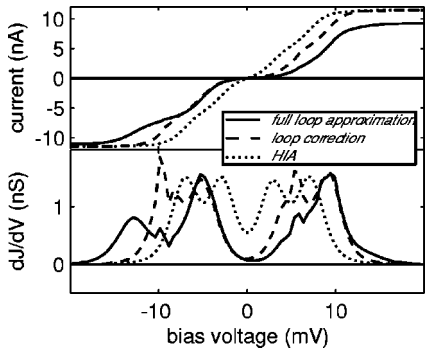

FIG. 7. *J-V* characteristics (upper panel) and dJ/dV (lower panel) for the DQD calculated in the full loop approximation (solid), with the loop correction (dashed) and within the HIA (dotted). Parameters are taken from case (A) in Table I.

A. Asymmetric current-voltage

An example of the *J-V* characteristics and corresponding dJ/dV for the DQD system with parameters according to the configuration listed in Table I (A) is shown in the upper and lower panels of Fig. 7, respectively. First we note that the two currents in the two mean field approximations, HIA (dotted) and loop correction (dashed), are shifted in the sense that the two transitions become resonant at lower bias voltages in the HIA than in the loop correction. This is understood from the discussion of the renormalization of the transition energies in Sec. III A, since it tends to push the transition energies deeper below the equilibrium chemical potential of the system. Naturally then the peaks in the dJ/dV calculated within the HIA appear at lower fields than the corresponding peaks in the loop correction. The loop correction gives rise to a slight asymmetry of the magnitude of the peaks in the dJ/dV curve, where the first peak for forward-bias voltages (around 5 mV) is a little bit lower than the second. For backward-bias voltages the situation is the opposite. This behavior is also understood from the asymmetric renormalization of the transition energies, see Fig. 5. However, the effect on the resulting current from this asymmetric renormalization is negligible.

When the dressing of the end-factors are included into the calculations, i.e., the full loop approximation (solid), the asymmetry of the *J-V* characteristics as well as the dJ/dV

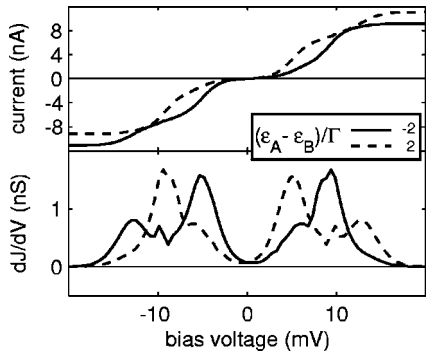

FIG. 8. Symmetry of the *J-V* characteristics and dJ/dV with respect to the relative positions of the levels in the QDs. The plots are calculated for $t/\Gamma=1$.

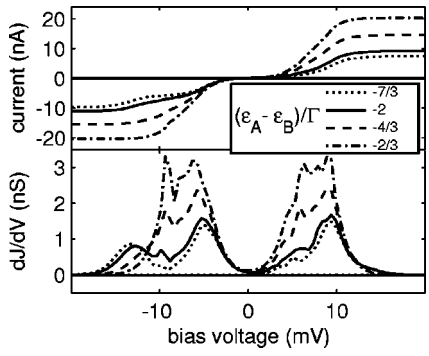

FIG. 9. *J-V* characteristics and dJ/dV for different relative level spacing $(\varepsilon_A-\varepsilon_B)/\Gamma<0$ in the two QDs and fixed hopping strength $(t/\Gamma=1)$ between the QDs.

curve becomes obvious. Consider the backward-biased system at first. The large increase of the current seen in the loop correction in the range -3 to -7 mV, remains in the full loop approximation, since the spectral weights are almost equal down to about -7 mV in the two cases. However, as the bias voltage approaches the range where the dynamical effects of the dressed end-factors become important, the current does not increase in a step-like fashion. The dJ/dV shows a double peak with a small amplitude and a minimum around -11 mV, which is where the dressed population number N_1 has its corresponding minimum, cf. Fig. 6(b). Similarly for forward-bias voltages, the amplitude of the step around 5 mV is less in the full loop approximation than in the loop correction, which is understood as an effect of the scattering between the one-particle states causing a decreased probability for electrons to undergo the transition $|\gamma_{2\sigma}\rangle\langle 0|$ in the DQD. Hence, the resulting currents in the three different approximations, can be understood from the discussion about the population numbers of the transitions between the empty state and the one-particle states in the previous section. Having analyzed the difference of the three approximation schemes, we now proceed to investigate the resulting currents through the DQD in the full loop approximation.

The relative positions of the discrete levels in the two QDs are of main importance in order to understand the asymmetry of the *J-V* characteristics of the system, as was pointed out in Sec. II. When the two levels are aligned, the transition matrix elements $(d_{A\sigma})^{0\gamma_{n\sigma}}$ and $(d_{B\sigma})^{0\gamma_{n\sigma}}$, $n=1,2$, are equal. As the difference $\varepsilon_A-\varepsilon_B<0$, the lower DQD orbital couples strong/weak to the left/right contact, whereas the upper orbital couples strong/weak to the right/left contact. In the case of $\varepsilon_A-\varepsilon_B>0$, the couplings of the DQD orbitals to the left and right contacts become the opposite. Thus it is expected that the *J-V* characteristics should be mirrored with respect to the difference $\varepsilon_A-\varepsilon_B$. By varying the difference $\varepsilon_A-\varepsilon_B$ for fixed coupling strengths to the left/right contacts, we see in the upper panel of Fig. 8 that this is indeed the case. For a negative difference (solid), e.g., $(\varepsilon_A-\varepsilon_B)/\Gamma<0$, the current flattens for *negative* bias voltages around $2\Delta_{\gamma_{1\sigma}}$, whereas in the opposite case (dashed), e.g., $(\varepsilon_A-\varepsilon_B)/\Gamma>0$, the current flattens for *positive* bias voltages around $-2\Delta_{\gamma_{1\sigma}}$. The corresponding dJ/dV plots show perfect reflections of one another, as is seen in the lower panel of Fig. 8. Clearly, it is sufficient to further analyze the case of $(\varepsilon_A-\varepsilon_B)/\Gamma<0$ (or $(\varepsilon_A-\varepsilon_B)/\Gamma>0$) only.

Now, consider varying the relative level spacing, $(\varepsilon_A-\varepsilon_B)/\Gamma<0$. From Fig. 4 we see that when the levels in the two QDs are aligned, the transition matrix elements $|(d_{A\sigma})^{0\gamma_{n\sigma}}|^2=|(d_{B\sigma})^{0\gamma_{n\sigma}}|^2$, $n=1,2$, which leads to a symmetric *J-V* curve since the coupling of the transitions $|\gamma_{n\sigma}\rangle\langle 0|$ to the left and right contacts are equal. For a finite relative level spacing, the transition matrix elements become distinct, for all values of the hopping t. Thus, the asymmetry imposed on the system will provide an asymmetric *J-V* (dJ/dV) characteristics, which is clearly seen in Fig. 7. In the upper (lower) panel of Fig. 9 we illustrate the increasing asymmetry of the *J-V* (dJ/dV) characteristics with respect to an increasing relative level spacing, for a fixed hopping t/Γ. As is seen, the current is only slightly asymmetric for small values of $(\varepsilon_A-\varepsilon_B)/\Gamma$, whereas the asymmetry increases with increasing level spacing. This clearly demonstrates the large influence of the scattering between the one-particle states as a result of the enlarged degree of asymmetric coupling to the left/right contacts, due to the growing level spacing.

Next, we let the relative level spacing be fixed and vary the hopping t/Γ. From Fig. 4 it is clear that the degree of asymmetry is large for low hopping rates, whereas for high hopping rates the asymmetry is somewhat smaller. This is clear, since the transition matrix element $|(d_{A\sigma})^{\gamma_{n\sigma}0}|^2=|u^{\sigma}_{n1}|^2 \to 1/2$ in the limit $t\to\infty$ for any relative level spacing such that $(\varepsilon_A-\varepsilon_B)/t\to 0$. Thus, one would expect that the asymmetry of the *J-V* characteristics becomes small for high tunneling probabilities between the QDs. This is clearly seen in Fig. 10, which displays the current (upper panel) and differential conductance (lower panel) for various hopping strengths t/Γ. One should note that a large hopping results in a large separation of the transition energies $\Delta_{1\sigma}$, which eventually leads to that $\Delta_{2\sigma}$, cf. Fig. 3(b), becomes positive for increasing t/Γ. This is the case for $t/\Gamma=5$ (dash-dotted) in Fig. 10, showing that $\Delta_{2\sigma}$ lies in the vicinity of the equilibrium chemical potential, μ, which gives a high conductance for low bias voltages. Nevertheless, the plots in Fig. 10 demonstrate that the system, hence the resulting current, becomes increasingly asymmetric as $t/\Gamma\to 0$ and decreasingly asymmetric as $t/\Gamma\to\infty$.

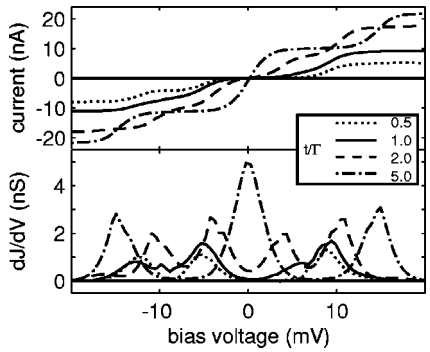

FIG. 10. *J-V* characteristics and dJ/dV for different hopping strengths t/Γ and fixed level spacing $(\varepsilon_A-\varepsilon_B)/\Gamma=-2$.

Both in Figs. 9 and 10 it is seen that the amplitude of the current tends to increase as the system becomes more and more symmetric, i.e., the transition matrix elements $|(d_{A\sigma})^{0}\gamma_{n\sigma}|^2, |(d_{B\sigma})^{0}\gamma_{n\sigma}|^2 \rightarrow 1/2$, $n=1,2$. This is expected since an equally strong coupling of the transition $|\gamma_{n\sigma}\rangle\langle 0|$ with respect to the left and right contacts means that the corresponding DQD orbital extends with uniform probability amplitude throughout the DQD. As the DQD becomes strongly asymmetric, in the sense that the transition matrix elements approaches 1 or 0, one finds a large probability amplitude of the orbital in one of the QDs and a small in the other one, as discussed in Sec. II. The conductivity of the DQD is closely related to this fact, since a strong localization of a state in one of the QDs yields a weak tunneling probability through the other, hence the overall current is reduced.

In experiments, it is rather difficult to establish a perfect symmetry of the tunnel barriers between the DQD with respect to the left and right contacts,[34–37] which means that the couplings $\Gamma^{L/R}$ are distinct. Motivated by this, we have also studied the additional effect on the *J-V* (dJ/dV) asymmetries arising due to the *external* asymmetric coupling, shown in Fig. 11 for two asymmetric couplings which are compared to the case of symmetric couplings. However, due to the finite level spacing and low hopping rate there is an *internal* asymmetry of the DQD, as previously discussed. One notes that a strong coupling to the left contact ($\Gamma^R/\Gamma^L<1$) amplifies the internal asymmetry of the DQD resulting in a further increased asymmetry of the *J-V* (dJ/dV) characteristics. The opposite case, e.g., $\Gamma^R/\Gamma^L>1$, tends to force the system into a more symmetric behavior, with respect to the bias voltage. The external asymmetry, however, does not substantially modify the current for either case, as is seen in Fig. 11. It should be emphasized, that any mean field result (that does not account for level shifts as functions of the bias voltage) would give perfectly symmetric *J-V* (dJ/dV) characteristics for all cases considered in Fig. 11. Hence, we conclude that the *J-V* (dJ/dV) asymmetries arise due to scattering between the DQD states. The effects from these scattering processes become amplified by the strong localization of the DQD orbitals to one of the QDs, as a result of the relative level spacing in the two QDs and the strongly correlated electron states within the DQD.

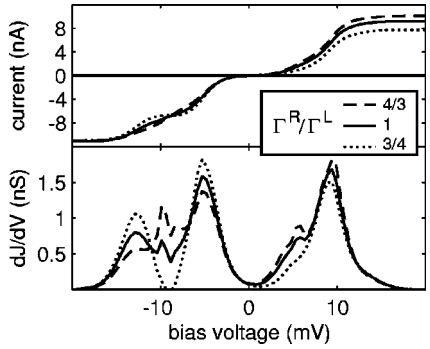

FIG. 11. *J-V* characteristics and dJ/dV for various left and right couplings Γ^L/Γ^R given the hopping strength $t/\Gamma=1$ and level spacing $(\varepsilon_A-\varepsilon_B)/\Gamma=-2$.

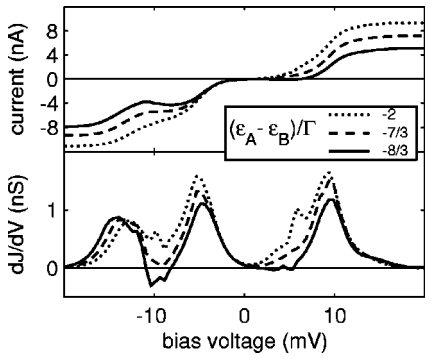

FIG. 12. *J-V* characteristics and dJ/dV for increasing relative level spacing $(\varepsilon_A-\varepsilon_B)/\Gamma$ given a fixed hopping rate $t/\Gamma=1$. Note that the solid *J-V* curve is the same as one given in Fig. 1.

B. Negative differential conductance

In this subsection we address the question of the asymmetric NDC, recently found in experiments.[10] In order to do this, we capture the main important property of the two carbon nano-tubes (CNTs), coupled via a SiO_2 tunnel barrier, as described in the experimental work of Ref. 10, namely, the level quantization. It should be noted that, the CNTs may suffer from various anisotropy effects and other conditions, which we neglect here. The level separation in the experimental CNT is of the order of $\sim$10 meV and the intra-CNT Coulomb repulsions are at least in this order. Thus, for sufficiently low bias voltages it is appropriate to adopt the model for the DQD given in Eq. (1), with one conducting level in each QD, and thus the developed theory in Sec. III. By using this approach we can directly study the interactions that give rise to the observed NDC.

From the lower panel in Fig. 9, it is clear that the double peaks appearing for negative bias voltages separate as the relative level spacing $(\varepsilon_A-\varepsilon_B)/\Gamma$ grows. Simultaneously, the valley between the peaks approaches zero conductance. Hence, from this picture the first requirement, for a region of NDC to appear in the *J-V* (dJ/dV) characteristics, is to increase the relative level spacing $(\varepsilon_A-\varepsilon_B)/\Gamma$. The second requirement is a low hopping rate, t/Γ, which was illustrated in Fig. 10. For a fixed hopping rate and increasing relative level spacing, we find that this is indeed the case, as is leg-

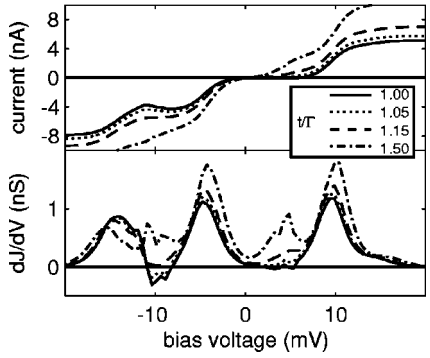

FIG. 13. *J-V* characteristics and dJ/dV for increasing hopping rate t/Γ given a fixed relative level spacing $(\varepsilon_A-\varepsilon_B)/\Gamma=-8/3$.

ible in Fig. 12. Here, the couplings $\Gamma^R/\Gamma^L=1$. In Sec. IV A it was suggested that the *J-V* asymmetries arise due to a substantial decrease of the population number N_1, resulting in that the transition $|\gamma_{1\sigma}\rangle\langle 0|$ becomes less available for conduction. By the same argument, the NDC is the result of a further decreased availability, eventually completely blocking any conduction through the DQD via $|\gamma_{1\sigma}\rangle\langle 0|$. In the lower panel of Fig. 12, it is seen how the valley between the two conductance peaks evolve from being positive to negative as the relative level spacing grows, for negative bias voltages. The transition $|\gamma_{1\sigma}\rangle\langle 0|$ starts to conduct for bias voltages slightly below its corresponding resonance value, due to the finite width of the transition. For increasingly (negative) values of the bias voltage, the conductance of the transition drops and, eventually, becomes more or less unavailable for conducting electrons through the DQD, hence, the current drops. A further increased (negative) bias voltage results in a reestablished conduction through the DQD via $|\gamma_{1\sigma}\rangle\langle 0|$, hence the current grows again. The small NDC around 5 mV is most likely due to numerical errors in the numerical differentiation, since the current is vanishingly small in this range of bias voltages.

Small hopping rates t/Γ between the QDs tend to preserve the asymmetric properties of the DQD whereas larger values of t/Γ forces the system in to a more symmetric performance, as discussed in Sec. IV A. This fact is confirmed by noting that the region of NDC vanish for growing t/Γ, as seen in Fig. 13, which is calculated for a fixed relative level spacing and symmetric couplings $(\Gamma^R/\Gamma^L=1)$.

V. SUMMARY AND CONCLUSIONS

In summary, we have studied the transport properties of a DQD coupled to external contacts, with respect to *internal* asymmetries resulting from the relative level spacing $\varepsilon_A-\varepsilon_B$ and the hopping rate t between the QDs. By expressing the DQD in terms of its exact many-body eigenstates (in the atomic limit), it was found that the transitions between the empty state and the one-particle states were asymmetrically coupled to the left and right contacts, for finite relative level spacing and hopping rate. A theory for *J-V* (dJ/dV) asymmetries was developed, beyond mean field theory, showing that the internal asymmetries give rise to an amplification of the effect of the dynamical (bias voltage dependent) redistribution of the spectral weights for these transitions. This results in a decreased probability amplitude for the transitions at bias voltages corresponding to their resonance values. The *J-V* (dJ/dV) characteristics was analyzed as a function of the relative level spacing and hopping rates. It was found that a large relative level spacing $|\varepsilon_A-\varepsilon_B|/\Gamma\gtrsim 2$, where $\Gamma=\Gamma^L+\Gamma^R$ is the sum of the couplings to the left and right contacts, gives a noticeably asymmetric *J-V* (dJ/dV) characteristics, for small hopping rates $t/\Gamma\lesssim 1$. The *J-V* (dJ/dV) characteristics show a region of NDC at one half of the range of bias voltages, for sufficiently large relative level spacing $(|\varepsilon_A-\varepsilon_B|/\Gamma\gtrsim 8/3$, given $t/\Gamma\sim 1)$. This behavior is in good agreement with the recent experimental finding on DQDs constructed from a CNT with a SiO_2 tunnel barrier deposited on the nano-tube.[10]

Experiments on DQD where the relative level spacing (and possibly the hopping rate) can be varied would be very intriguing, and would provide valuable information to reach a better understanding of the asymmetric transport properties of nano-devices.

ACKNOWLEDGMENTS

Valuable discussions with I. Sandalov are acknowledged. J.F. also thanks V. Cheianov, A. Luther, and S. Mirbt for encouraging and helpful comments. Support from Göran Gustafsson's foundation, the Foundation for Strategic Research (SSF) and Swedish National Science Foundation (VR) is acknowledged.

*Electronic address: Jonas.Fransson@fysik.uu.se

[1] M. A. Reed, C. Zhou, C. J. Muller, T. P. Burgin, and J. M. Tour, Science **278**, 252 (1997).

[2] J. Reichert, R. Ochs, D. Beckmann, H. B. Weber, M. Mayor, and H. v. Löhneysen, Phys. Rev. Lett. **88**, 176804 (2002).

[3] J. Reichert, H. B. Weber, M. Mayor, and H. v. Löhneysen, Appl. Phys. Lett. **82**, 4137 (2003).

[4] J. Leo and A. H. MacDonald, Phys. Rev. Lett. **64**, 817 (1990).

[5] D. K. Ferry and S. M. Goodnick, *Transport in Nanostructures* (Cambridge University Press, Cambridge, 1997).

[6] A. Zaslavsky, V. J. Goldman, D. C. Tsui, and J. E. Cunningham, Appl. Phys. Lett. **53**, 1408 (1988).

[7] T. Schmidt. M. Tewordt, R. J. Haug, K. von Klitzing, A. Förster, and H. Lüth, Solid-State Electron. **40**, 15 (1996).

[8] G. Klimeck, R. Lake, S. Datta, and G. W. Bryant, Phys. Rev. B **50**, 5484 (1994).

[9] W. Rudziński and J. Barnaś, Phys. Rev. B **64**, 085318 (2001).

[10] K. Ishibashi, M. Suzuki, T. Ida, and Y. Aoyagi, Appl. Phys. Lett. **79**, 1864 (2001).

[11] T. C. L. G. Sollner, W. D. Goodhue, P. E. Tannenwald, C. D.

Parker, and D. D. Peck, Appl. Phys. Lett. **43**, 588 (1983).
[12] A. Sibille, J. F. Palmier, H. Wang, and F. Mollot, Phys. Rev. Lett. **64**, 52 (1990).
[13] R. Tsu and L. Esaki, Appl. Phys. Lett. **22**, 562 (1973).
[14] L. L. Chang, L. Esaki, and R. Tsu, Appl. Phys. Lett. **24**, 593 (1974).
[15] N. C. van der Vaart, S. F. Godjin, Y. V. Nazarov, C. J. P. M. Harmans, J. E. Mooij, L. W. Molenkamp, and C. T. Foxon, Phys. Rev. Lett. **74**, 4702 (1995).
[16] W. G. van der Wiel, S. De Franceschi, J. M. Elzerman, T. Fujisawa, S. Tarucha, and L. P. Kouwenhoven, Rev. Mod. Phys. **75**, 1 (2003).
[17] M. R. Wegewijs, Y. V. Nazarov, and S. A. Gurvitz, Jpn. J. Appl. Phys., Part 1 **40**, 1994 (2001).
[18] R. López, R. Aguado, and G. Platero, Phys. Rev. Lett. **89**, 136802 (2002).
[19] T.-S. Kim and S. Hershfield, Phys. Rev. B **63**, 245326 (2001).
[20] Y. Takazawa, Y. Imai, and N. Kawakami, J. Phys. Soc. Jpn. **71**, 2234 (2002).
[21] C. Lacroix, J. Phys. F: Met. Phys. **11**, 2389 (1981).
[22] S. Hershfield, J. H. Davies, and J. W. Wilkins, Phys. Rev. Lett. **67**, 3720 (1991).
[23] J. Fransson, O. Eriksson, and I. Sandalov, Photon. Nanostruct. (to be published).
[24] J. Hubbard, Proc. R. Soc. London, Ser. A **276**, 238 (1963).
[25] J. Hubbard, Proc. R. Soc. London, Ser. A **277**, 237 (1963).
[26] Y. Meir and N. S. Wingreen, Phys. Rev. Lett. **68**, 2512 (1992).
[27] A.-P Jauho, N. S. Wingreen, and Y. Meir, Phys. Rev. B **50**, 5528 (1994).
[28] J. Fransson, O. Eriksson, and I. Sandalov, Phys. Rev. B **66**, 195319 (2002).
[29] J. Fransson, O. Eriksson, and I. Sandalov, Phys. Rev. Lett. **88**, 226601 (2002).
[30] I. Sandalov, B. Johansson, and O. Eriksson, Int. J. Quantum Chem. **94**, 113 (2003).
[31] I. Sandalov, U. Lundin, and O. Eriksson, cond-mat/0011260 (2001).
[32] J. Fransson, E. Holmström, O. Eriksson, and I. Sandalov, Phys. Rev. B **67**, 205310 (2003).
[33] D.C. Langreth, in *Linear and Nonlinear Electron Transport in Solids*, Vol. 17 of *NATO Advanced Study Institute*, *Series B: Physics*, edited by J. T. Devreese and V. E. van Doren (Plenum, New York, 1976).
[34] M. Saitoh, T. Saito, T. Inukai, and T. Hiramato, Appl. Phys. Lett. **79**, 2025 (2001).
[35] T. Junno, S.-B. Carlsson, H. Q. Xu, L. Samuelsson, A. O. Orlov, and G. L. Snider, Appl. Phys. Lett. **80**, 667 (2002).
[36] Y. Shimada, K. Hirakawa, M. Odnoblioudov, and K. A. Chao, Phys. Rev. Lett. **90**, 046806 (2003).
[37] C. Thelander, T. Mårtensson, M. T. Björk, B. J. Ohlsson, M. W. Larsson, L. R. Wallenberg, and L. Samuelsson, Appl. Phys. Lett. **83**, 2052 (2003).